Eur. Phys. J. B **28**, 305–313 (2002)
DOI: 10.1140/epjb/e2002-00234-6

THE EUROPEAN PHYSICAL JOURNAL B

Reactivity and magnetism of Fe/InAs(100) interfaces

C.M. Teodorescu[1,a], F. Chevrier[2], R. Brochier[3], C. Richter[3], V. Ilakovac[3], O. Heckmann[3], P. De Padova[4], and K. Hricovini[3]

[1] National Institute for Research and Development in Materials Physics, Bucharest-Magurele PO Box MG7, 76900 Romania
[2] LURE, bâtiment 209d, Centre Universitaire Paris-Sud, BP 34, 91898 Orsay Cedex, France
[3] LPMS, Université de Cergy-Pontoise, 95031 Cergy-Pontoise Cedex, France
[4] CNR-ISM, via Fosso del Cavaliere, 100, 00133 Roma Italy

Received 4 April 2002 / Received in final form 13 May 2002
Published online 31 July 2002 –

Abstract. Interface reaction and magnetism of epitaxially-grown Fe on InAs(100) are studied by core-level photoemission (As 3*d* and In 4*d*) and Fe 2*p* X-ray magnetic circular dichroism using synchrotron radiation. The reactivity of Fe/InAs(100) is relatively low compared to that of other interfaces involving deposition of 3*d* metals on III-V semiconductors. As a consequence, we observe a magnetic signal at Fe $L_{2,3}$ edges for the lowest thicknesses studied (1 ML). The atomic magnetic moment reaches a value close to that of the bulk α-Fe (2.2 μ_B) for Fe coverages exceeding 5 ML. A ferromagnetic compound with approximate stoichiometry of FeAs is formed at the interface. The orbital magnetism represents between 12 and 20% of the total momentum, due to 3*d* density of states depletion and to crystal-field modification of the electronic levels. These properties make the Fe/InAs(100) interface very promising for spin-tunneling devices.

PACS. 61.10.Ht X-ray absorption spectroscopy: EXAFS, NEXAFS, XANES, etc. – 68.35.Fx Diffusion; interface formation – 75.70.Ak Magnetic properties of monolayers and thin films – 82.80.Pv Electron spectroscopy (X-ray photoelectron (XPS), Auger electron spectroscopy (AES), etc.)

1 Introduction

Magnetism of transition metals grown on semiconductors has attracted special interest during the last two decades since these structures open new possibilities yet unexploited in microelectronics [1]. Among these possibilities, spin injection devices, which offer the possibility of a high-degree control of the tunneling current by means of applied magnetic fields [2], occupy a central role. One of the most important properties of interfaces used for spin injection processes concerns the *orbital magnetism* since it was recognized that the itinerant *d* states are the major component of the tunneling current [3].

However, to date only a few X-ray magnetic circular dichroism (XMCD) results were reported on these interfaces, although this technique is able to separate between spin and orbital magnetism through well-known sum rules [4]. XMCD on Fe/GaAs(100) showed a huge increase of about three times of the Fe orbital magnetic moments [5] and this increase was attributed to the localization of 3*d* states due to the presence of surface roughness and of interdiffusion [6]. In the present contribution we present new results from XMCD on 3*d* metals grown on III-V semiconductors and considerations about the origin of the orbital moment enhancement.

Of the 3*d* metal / III-V semiconductor interfaces the most studied is Fe/GaAs [7–9] since it implies the use of the most magnetic 3*d* metal grown on the most commonly used semiconductor material of this class. The properties of this interface can be summarized as follows: (i) the interface is strongly reactive, metal deposition induces interface disruption, formation of interface $FeGa_xAs_y$ compounds, diffusion of Ga and As through the Fe layer, and segregation of As at the surface [7]; (ii) the magnetism of Fe layers is reduced; for very thin films of less than 10 Fe atomic layers the magnetic moment per atom (MMA) is about 50% of the MMA of bulk bcc Fe (approximately 1.1 μ_B [8]); (iii) the formation in some cases at the interface of a magnetically dead layer of 5–6 Fe monolayers (ML) [8]; below this Fe coverage no magnetism is detected [9]. More recent work established a critical thickness for the onset of the ferromagnetic order of 3.5 ML [5,10], with the ferromagnetic polarisation of the whole amount of Fe when the coverage exceeds this critical thickness due to Fe cluster percolation. All these properties reduce the potential of possible applications and suggest needs for the study of other interfaces.

In addition, Fe forms a rectifying contact on GaAs leading to a Schottky barrier height of about 0.8 eV,

[a] *Present address:* Magnetic Spectroscopy, Daresbury Laboratory, Daresbury, Warrington, Cheshire WA4 4AD, UK
e-mail: C.Teodorescu@dl.ac.uk

which prevents efficient spin injection into the semiconductor [11–13]. Recent work on Fe/AlGaAs interface [14] has achieved a spin injection efficiency of 30% by a careful choice of the doping profile of the top AlGaAs layer such that the Schottky contact had a narrow depletion width and forms a triangular shaped tunnel barrier. However, it appears interesting also to study 3*d* metals deposited on narrow gap and high carrier mobility semiconductors, such as InAs with a direct band gap as small as 0.36 eV at 300 K [13]. Recently it was demonstrated that in spite of the large mismatch (5.4%) between twice the lattice constant of Fe (2.866 Å) and that of InAs (6.058 Å), bcc Fe can be stabilized on InAs(100) and exhibits magnetic properties [11,15–18]. The aim of the present study is to extend the analysis of the properties of Fe/InAs(100) by addressing the points (i–iii) mentioned above, if possible, in a quantitative way. We investigated the interface chemistry by photoelectron spectroscopy (PES) and the magnetism by Fe $L_{2,3}$ XMCD.

2 Experimental

The experiments are performed in a UHV chamber equipped with a VSW hemispherical electron spectrometer and a magnetic field (±400 Oe = 0.04 T) supply, connected to a molecular beam epitaxy (MBE) installation where the samples are prepared and to the SU23 beamline at the Super Aco storage ring in Orsay (70% of circular polarization). All chambers operate in low 10^{-10} mbar pressure range. For XMCD, absorption spectra are recorded with the circular polarization vector of the X-rays either parallel or antiparallel to the applied magnetic field by using the total electron yield (TEY) method [19]. The XMCD signal is defined as the difference of the two absorption spectra $\mu_+ - \mu_-$ and further corrected by $1/\cos\alpha_0$, where α_0 is the angle between the magnetic field vector and the easy magnetization axis of Fe [110] [16,18]. As 3*d* and In 4*d* PES spectra are recorded with a photon energy of 200 eV, in order to get essentially surface and interface contribution. The photoelectron escape depth at the respective kinetic energies is estimated to around 7–8 Å. All measurements presented here (PES and XMCD) were performed at room temperature.

InAs(100) *c* 8×2 were obtained by Ar sputtering and annealing. Fe films were grown in the MBE chamber at rates around 1 Å / min on the substrate held at 450 K [16] and subsequently characterized by reflectance high energy electron diffraction (RHEED), Auger and X-ray photoelectron (XPS) spectroscopies. No C or O contamination were detected by Auger or XPS. The Fe coverage was determined by using a quartz microbalance and periodically checked by Auger spectroscopy, XPS and RHEED oscillations of Fe/V(100). The typical error in coverage determination is estimated to ±5%. Each sample was freshly prepared. The RHEED and XPS spectra are subject of a former communication [17]. In the above conditions, one observes nearly layer-by-layer growth with a quick relaxation of the lattice parameter to that of Fe for a few monolayers. From the intensity of the Al K_α excited XPS peaks (As 2*p* and In 3*d*) we derived that approximately 1 ML of As is floating on the top of the Fe film even for the thickest films investigated (≈ 36 ML) whereas the In signal is exponentially attenuated.

3 Results and discussion

3.1 Core-level photoemission

3.1.1 In 4d and As 3d core-level photoemission

Figure 1 presents In 4*d* and As 3*d* intermediate-resolution electron distribution curves (EDCs). The overall Gaussian full width at half maximum, responsible for beamline and electron spectrometer instrumental broadening, was determined to be 200 ± 20 meV. The nominal coverage of Fe is expressed in ML with respect to bulk bcc Fe (1 ML = 1.433 Å). Both core level EDCs can be well decomposited into two components, one which is attributed to the bulk component and another which is attributed to In and As atoms reacted at the interface. The fit was performed using Voigt profiles and their integrals for the inelastic background [20] as follows: firstly all parameters were allowed to vary with starting parameters set randomly. Then, the branching ratio (BR), the spin-orbit splitting (SOS) and the Lorentzian width (LW) were fixed to the average value obtained from all trials and all EDCs (BR = 1.500, identical to the theoretical value; LW = 0.164 eV for As 3*d* and 0.193 eV for In4*d*; SOS = 0.7 eV for As 3*d* and 0.87 eV for In 4*d*; all values are in good agreement with those reported previously [12]). No improvement of the quality of the fit was observed by unblocking these parameters. The relevant fitting variables were: the Gaussian width, the inelasting background amplitude, the amplitudes and energies of the $3d_{5/2}$ lines.

Interestingly, although clear 8×2 RHEED patterns were visible, the clean substrate EDCs were well fitted with only one component. This seems to indicate that the energy position of the surface In and As adatoms is very close to that of bulk atoms. We did not detect any concludent shift in the binding energy of the bulk component upon Fe deposition. As soon as Fe is deposited, the bulk components decrease and interface components appear. These components are shifted with respect to bulk components by around 0.95 eV towards higher binding energy for As, and by around 0.42 eV towards lower binding energies for In. If we assume that the In-As bond in the solid has a partial ionic character $In^{\delta+}As^{\delta-}$ ($\delta \approx 0.2$ [21]), the results of the above analysis imply that in the reacted layer the In and As atoms are more neutral.

3.1.2 Data interpretation

These results should be compared with those of the widely studied interface Fe/GaAs [7]. Here one observes the occurence of a reacted component shifted by around 1 eV towards lower binding energy for Ga, and of two reacted components shifted by around 0.4 and 0.7 eV towards

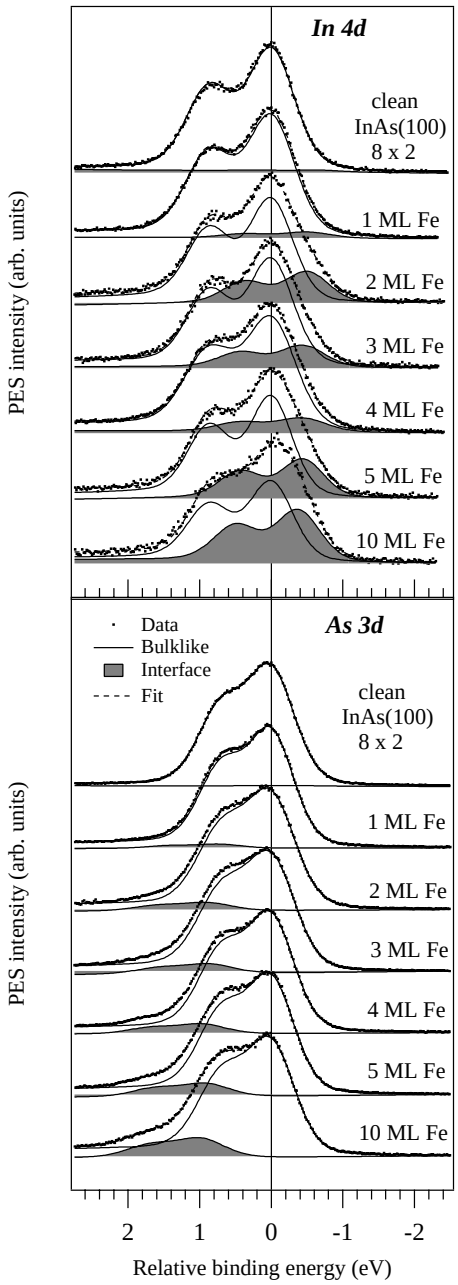

Fig. 1. In 4*d* and As 3*d* electron distribution curves. The dashed components represent contributions from reacting In and As.

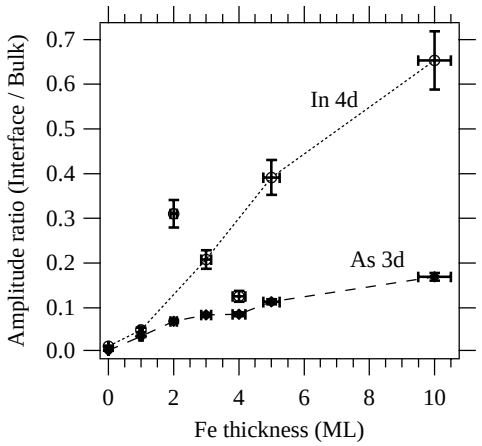

Fig. 2. Ratios between In 4*d* and As 3*d* interface and substrate components, as function of Fe coverage.

lower binding energy for As. The main differences between Fe/GaAs and Fe/InAs (the present study) need to be emphasized: (i) the extent of the reaction is much lower in Fe/InAs than in Fe/GaAs; (ii) the reacted As is represented by only one 3*d* component which is shifted towards *higher* binding energy; (iii) the shift of the reacted In 4*d* component in Fe/InAs is about one half of the shift of the reacted Ga 3*d* component in Fe/GaAs; (iv) the reaction seems to be mainly Fe-In driven whereas for Fe/GaAs it is Fe-As driven. However, the last statement should be considered with care. As will be discussed below, the "bulk" component of the As 3*d* peak contains contributions from As atoms which have reacted with Fe and are a in ionization state close to that of As into bulk InAs.

XPS experiments have shown that about 1 ML of As is floating at the surface [17]. Taking into account the present data, we can affirm that this quantity of As (the interface component from Fig. 1) is neutral [12,22]. Scanning tunneling microscopy (STM) experiments have shown the presence of extended In islands while Fe is deposited. At this point, we can also remark that the binary phase diagram Fe-In do not show any intermediate compound [23] whereas the phase diagram Fe-Ga shows several compounds ($\alpha, \beta-$ Fe_3Ga, $\alpha, \beta-$ Fe_6Ga_5, Fe_3Ga_4, and $FeGa_3$) [24]. Therefore, it is not surprising that at surface Fe and In regions are distinct and no intermediate compound is formed. The In atoms in these islands (interface component in Fig. 1) can also be considered as neutral.

The next point to be considered concerns the conservation of the number of As and In atoms that have been disrupted from the semiconductor interface. We assume that the photoelectron escape depth for the two core levels with 200 eV excitation energy is nearly the same; Figure 2 shows that the ratio between interface and the bulk In 3*d* component is about 4 times larger than the corresponding ratio for the As 3*d* core level. The interface As 3*d* component corresponds to 1 ML of As. If we then neglect effects due to different surface coverage by In or As, we could infer that about 4 ML of In are disrupted from the substrate. Thus, some 3 ML of As should react with Fe giving As atoms in a ionization state which is similar to that of bulk InAs and whose core level contribution cannot be separated from the bulk component. The Fe-As phase diagram shows stable $FeAs_2$, FeAs, and Fe_2As compounds [25] from which the last two are antiferromagnetic [26]). At this point we cannot infer which is exactly the stoichiometry of the interface Fe-As compound. It will be investigated below through the analysis of the magnetic properties of the interface, since it has

already been shown that $3d$ metal-As reactions lead to a reduction of the magnetic moment of the $3d$ metal [27].

Another comment concerns the magnitude of the ratios between the interface or floating (in the case of As) components and the bulklike ones. For instance, if 3 ML of As are reacting with Fe before this compound is covered by some other 7 ML of bulklike Fe, the ratio between the component representing the floating As and the bulklike As in the substrate and in the interface compound should yield $\lambda^{-1}\exp(7\text{ ML}/\lambda) = 0.8$ for the electron mean free path $\lambda = 5$ ML. These values are considerably larger than those represented in Figure 2. Explanations of this discrepancy rely on (i) a stronger interdiffusion of As into the Fe layer and/or (ii) the formation of Fe agglomerates, leaving parts of the surface free from deposited metal [15]. In the case of In, similar considerations give the ratio interface/bulk components as being ≈ 1.8 for the same value of λ. For both In and As, the ratio between the above estimated values and the experimental ones is about three to four. We suggest that new STM experiments should clarify which area of the substrate is effectively covered with Fe in the actual experimental conditions. The question of interdiffusion will be addressed in the following, when the magnetic properties of the Fe/InAs(100) heterostructures will be analyzed.

3.2 X-ray magnetic circular dichroism

3.2.1 Overview of the results

We examinate now the Fe $L_{2,3}$ absorption and XMCD results. In Figure 3 we present the isotropic absorption spectra and the integral of (background-subtracted) both $L_{2,3}$ white lines, as function of Fe coverage Θ. Owing to the finite escape depth of the detected electrons, to a good approximation, the points obey a saturation law:

$$I(\Theta) = I_0(1 - \exp(-\Theta/\lambda)) \qquad (1)$$

where λ is the electron mean free path. The fit (dashed curve in Fig. 3b) yields $\lambda = 5.31$ ML of Fe $= 7.61$ Å. This law can be used to scale the TEY signal with respect to the "true" absorption, proportional to the Fe coverage. Note that the above value of λ is far too low. The main component of the electrons detected by the TEY technique are secondary electrons produced by scattering of the fast Auger electrons into the sample [28]. The escape depth of these low-energy electrons is estimated from the study of interfaces presenting well-defined layer-by-layer growth such as Fe/V(100), Ni/Cu(100), etc. to be around 17 Å, in good agreement with reference [29]. This discrepancy will be clarified in the following.

The XMCD signal (XMCD $= \mu_+ - \mu_-$) is represented in Figure 4 (before correction by circular polarization and angular factors). As expected, it increases with increasing Fe coverage, but let us remark that a non-vanishing XMCD signal is present for the lowest Fe coverages investigated (1 ML) at room temperature. Therefore, we found ferromagnetic ordering of Fe at these low coverages, unlike the case of Fe/GaAs [5,8–10]. The detectable

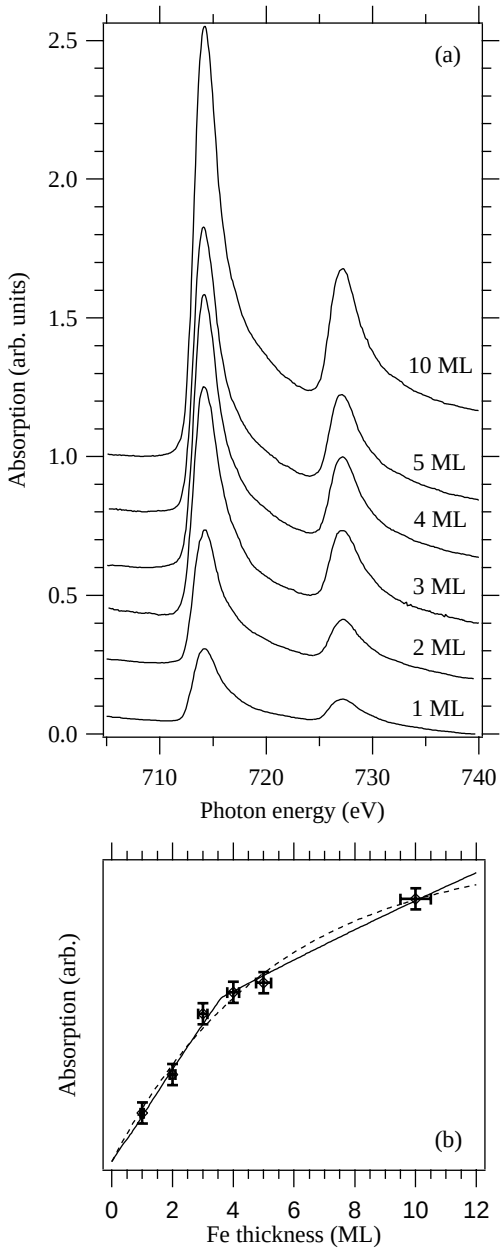

Fig. 3. (a) Fe $2p$ isotropic absorption spectra. (b) Dependence of $2p \rightarrow 3d$ integrated absorption on Fe coverage, with simulations using a simple saturation law with low electron mean free path (Eq. (1), dashed curve) or a three layer model with high electron mean free path (Eq. (3), full curve).

XMCD signal at very low coverages for the relatively low applied magnetic fields (400 Oe) means that ferromagnetic instead of superparamagnetic [15] ordering is present in the Fe films.

We applied the XMCD sum rules in order to derive the average values of spin and orbital components of the magnetic moment per Fe atom [4]. The XMCD spectra were integrated; from the isotropic absorption spectra

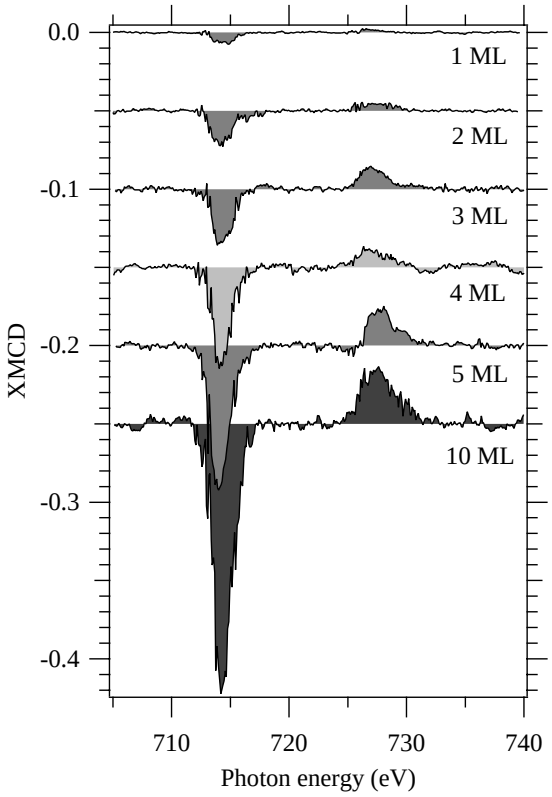

Fig. 4. Fe $2p$ X-ray magnetic circular dichroism, before correction from angular and polarisation factors (an overall factor of 2.75).

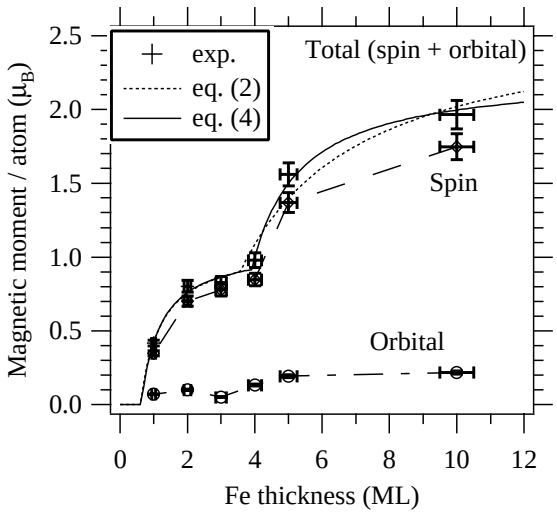

Fig. 5. Atomic magnetic moments per Fe atom, obtained by applying the XMCD sum rules. The total magnetic moment was fitted with a three layers model, represented in Figure 5 (see text for details).

(Fig. 2) the continuum contribution was subtracted, then they were integrated; finally, ratios between XMCD and absorption integrals provided the kinetic moments $\langle L_z \rangle$ and $\langle S_z \rangle$ ($\mu_{tot} = -\mu_B(\langle L_z \rangle + 2\langle S_z \rangle)$). We used the number of Fe $3d$ holes of 3.39, as reported previously [4]. In the spin magnetic moment sum rule, the dipolar magnetic term $\langle T_z \rangle$ was neglected, although this is known to cause errors in the case of low-dimensionality systems, in particular for noncubic symmetry [30]. As will be seen below, plausible results are obtained in this approximation and a possible explanation is that the early stages of Fe growth is characterized by 3D island formation [17,31] and by formation of an interface compound with cubic symmetry. Hence, no real "reduced-symmetry" (2D) interface is present and the dipole magnetic term seems to be quenched.

The net result of sum rules analysis is represented in Figure 5. As expected, the moments increase with the thickness of Fe film. This increase can be modelized by one- or two-step reaction.

3.2.2 Three-layer model of interface formation

It seems that up to about 4 ML of deposited Fe an interface layer with MMA lower than that of bulk Fe is formed; then, for increasing Fe coverages, a bulklike Fe phase is obtained on top. A simple model, drawn in Figure 6, supposes: (i) formation of a layer with very low MMA (M_1) of maximum Fe coverage Θ_1; then (ii) formation of a second layer with intermediate MMA (M_2), for $\Theta_1 < \Theta < \Theta_1 + \Theta_2$; (iii) growth of bulklike Fe with high MMA (M_{Fe}) for coverages exceeding $\Theta_1 + \Theta_2$.

The resulting MMA as function of Fe coverage $M(\Theta)$ is given by the weighted sum of MMA of Fe in the three different layers considered, as discussed also in reference [31]:

$$\begin{aligned} M(\Theta)\Theta &= M_1\Theta_1 \\ &\quad + M_2\Theta_2 + M_{\mathrm{Fe}}(\Theta - \Theta_1 - \Theta_2); \quad (\Theta > \Theta_1 + \Theta_2) \\ M(\Theta)\Theta &= M_1\Theta_1 + M_2(\Theta - \Theta_1); \quad (\Theta_1 + \Theta_2 > \Theta > \Theta_1) \\ M(\Theta) &= M_1; \quad (\Theta < \Theta_1). \end{aligned} \tag{2}$$

The fit using this equation is represented in Figure 5 (dashed curve). The resulting values are $M_1 = 0$, $M_2 = 1.08\ \mu_B$, $M_{\mathrm{Fe}} = 2.64\ \mu_B$, $\Theta_1 = 0.60$ ML, $\Theta_2 = 2.96$ ML. The overall agreement is good; nevertheless the MMA of the Fe film grown on top of the interface layer M_{Fe} exceeds largely the bulk value of bcc Fe ($2.2\ \mu_B$).

Taking into account also the escape depth of the detected electrons λ one needs to reformulate the $M(\Theta)$ dependence. Additional parameters in this dependence are Fe concentrations in the lower two layers a_1 and a_2 [31]. The corresponding layer thicknesses to be taken into account in the attenuation law of the electrons are $\Theta_{1,2}/a_{1,2}$ (Fig. 6). But, before modelizing the XMCD one needs to reformulate also the overall $2p$ absorption intensity

$$I(\Theta) = I_0^{(r)}\,[a_1 S_\lambda(\Theta_1/a_1)E_\lambda(\Theta-\Theta_1-\Theta_2)E_\lambda(\Theta_2/a_2) + a_2 S_\lambda(\Theta_2/a_2)E_\lambda(\Theta-\Theta_1-\Theta_2)] + I_0^{(Fe)} S_\lambda(\Theta-\Theta_1-\Theta_2);$$
$$(\Theta > \Theta_1+\Theta_2)$$
$$I(\Theta) = I_0^{(r)}\,[a_1 S_\lambda(\Theta_1/a_1)E_\lambda((\Theta-\Theta_1)/a_2) + a_2 S_\lambda((\Theta-\Theta_1)/a_2)]\,; \quad (\Theta_1+\Theta_2 > \Theta > \Theta_1);$$
$$I(\Theta) = I_0^{(r)} a_1 S_\lambda(\Theta/a_1); \quad (\Theta < \Theta_1). \tag{3}$$

$$M(\Theta) =$$
$$\frac{a_1 M_1 S_\lambda(\Theta_1/a_1)E_\lambda(\Theta-\Theta_1-\Theta_2)E_\lambda(\Theta_2/a_2) + a_2 M_2 S_\lambda(\Theta_2/a_2)E_\lambda(\Theta-\Theta_2) + M_{\mathrm{Fe}} I_0^{(Fe)}/I_0^{(r)} S_\lambda(\Theta-\Theta_1-\Theta_2)}{a_1 S_\lambda(\Theta_1/a_1)E_\lambda(\Theta-\Theta_1-\Theta_2)E_\lambda(\Theta_2/a_2) + a_2 S_\lambda(\Theta_2/a_2)E_\lambda(\Theta-\Theta_2) + I_0^{(Fe)}/I_0^{(r)} S_\lambda(\Theta-\Theta_1-\Theta_2)};$$
$$(\Theta > \Theta_1+\Theta_2)$$
$$M(\Theta) = \frac{a_1 M_1 S_\lambda(\Theta_1/a_1)E_\lambda(\Theta-\Theta_1) + a_2 M_2 S_\lambda((\Theta-\Theta_1)/a_2)}{a_1 S_\lambda(\Theta_1/a_1)E_\lambda(\Theta-\Theta_1) + a_2 S_\lambda((\Theta-\Theta_1)/a_2)}; \quad (\Theta_1+\Theta_2 > \Theta > \Theta_1);$$
$$M(\Theta) = M_1; \quad (\Theta < \Theta_1). \tag{4}$$

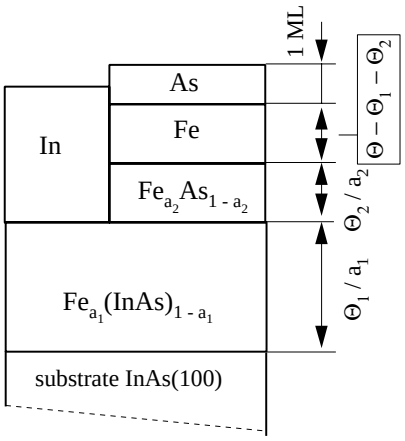

Fig. 6. Proposed structure for the reacted Fe/InAs(100) interface. The coverages Θ are related to the quantity of deposited Fe. Hence, the thickness of a layer whose Fe concentration is a is Θ/a.

dependence on the Fe coverage in the three layer model considered. The equation to be used is:

see equation (3) above.

In the above formula $E_\lambda(x) = \exp(-x/\lambda)$ and $S_\lambda(x) = (1-\exp(-x/\lambda))$. $I_0^{(\mathrm{Fe})}$ and $I_0^{(r)}$ are absorption intensities corresponding to bulk Fe and to Fe which has reacted with As. These two intensities are different, $I_0^{(\mathrm{Fe})} < I_0^{(r)}$, for the following reasons: firstly, Fe in coordination with As is in a positive ionization state; hence, the number of available $3d$ states increases. Secondly, in the presence of an anionic neighboring formed by $\mathrm{As}^{\delta-}$ the $3d$ Fe orbitals become more localized on the absorbing Fe atom. Hence, the overall Fe $2p \rightarrow 3d$ absorption cross section increases for Fe in the intralayers. The fit using equation (3) is also represented in Figure 3b (full curve). The relevant fitting parameters are $\lambda = 12$ ML $= 17$ Å, $\Theta_1 = 0.70$ ML, $\Theta_2 = 3.0$ ML, $a_1 \approx 0.05$, $a_2 = 0.5$.

We use these parameters as input for the simulation of the XMCD results. Escape depth effects and different absorption cross sections for the metal and the reacted Fe layers are taken into account by the following equation:

see equation (4) above.

The fit using equation (4) is also represented in Figure 5, continuous curve ($M_1 = 0$ and $\lambda = 12$ Å$= 17$ ML were fixed). Resulting values are $M_2 = 1.0\ \mu_B$, $M_{\mathrm{Fe}} = 2.3\ \mu_B$, $\Theta_1 = 0.70$ ML, $\Theta_2 = 3.0$ ML, $a_1 \approx 0.05$, and $a_2 = 0.50$. Remark that one obtains this time a value of the MMA for the Fe metal layer which is close to that of the bulk Fe ($2.2\ \mu_B$). Several fitting trials both of the Fe $2p$ absorption cross section (Fig. 3b) and of the effective MMA derived by sum rules (Fig. 5) yielded an estimate of the error bars: ± 0.05 for Fe concentrations $a_{1,2}$, ± 0.2 ML for effective coverages of the reacted layers $\Theta_{1,2}$, and $\pm 0.10 \mu_B$ for the momenta.

The interface evolution during Fe deposition can then be modelised as follows: (i) for coverages lower than about 0.6 ML, Fe atoms are diffusing into the substrate forming diluted $\mathrm{Fe}_x(\mathrm{InAs})_{1-x}$ ($x \approx 0.05$); (ii) for coverages between 0.7 and 3.7 ML, an interface compound is formed. From the PES results, about 3 ML of As are forming this reacted layer. The modelization of both $M(\Theta)$ and $I(\Theta)$ give a quantity of Fe of 3 ML participating to the formation of this layer with Fe dilution of 0.5 and MMA of about 1 μ_B. Consequently, it seems that a compound with approximate stoichiometry of FeAs is formed at the interface. The major difference with respect to bulk FeAs [26] is that this time FeAs is *ferromagnetic*. This should not be surprising in the presence of the topmost Fe magnetic layer which can polarise the intralayer; however, the interface FeAs is ferromagnetic even in the absence of the polarising outer layer. This effect could be related to a distortion of the FeAs induced by the large lattice spacing of InAs. Note here that the value of 1.06 μ_B obtained for the Fe atoms in the interface layer uses the number of $3d$ holes of 3.39 for the bulk Fe. FeAs should have a partly ionic character. From the PES position of the corresponding As component, which coincides with the position of

As in bulk InAs, a charge transfer of $0.2e$ from Fe to As could be inferred. Consequently, the number of $3d$ holes of Fe in FeAs increases to approximately 3.6 and the effective MMA per Fe atom derived from the above considerations has to be corrected by a factor of 1.06. At this point we can specify that trials to get an As XMCD signal at both $3p$ and $3d$ edges failed. Hence, no As magnetism is detected and the magnetism of the interface layer is driven just by the magnetism of Fe.

Finally (iii), for larger Fe coverages $\Theta > 3.7$ ML, bulk-like Fe with high magnetic moment grows on top of the interface compound.

Interestingly, the Fe coverage for the onset of metallic Fe growing derived here (3.7 ML) is sensibly close to the onset of Fe islands coalescence, as examinated by STM [11,15]. The majour difference between the present data and the previously-published results concerns the onset of the Fe ferromagnetic order instead of superparamagnetism for Fe coverages *lower* than 3.5 ML. This low-coverage behaviour may be caused by different substrate preparation: the actual experiments were performed on sputter-annealed InAs(100)c 8 $\times$2 substrates [17], whereas previous experiments [11,15,16,18] were performed on InAs(100) c 4 $\times$ 2. Template effects have been recognised to play an important role in the structural and magnetic properties of the grown films [32]. In some cases, films with similar magnetic properties are obtained on different substrate reconstructions [9], but this is not a general rule. Surface roughness also affect the magnetic properties [6]. In the early stages of Fe film growth, we could think about the formation of extended FeAs ferromagnetic regions in the present case, compared with formation of 3D Fe superparamagnetic clusters in the case of InAs(100) c 4 $\times$ 2 substrates. One possible origin of this different behaviour could be that the c 8 $\times$ 2 surface is more flat than the c 4 $\times$ 2 one, therefore favourising layer-by-layer growth.

3.2.3 Enhancement of orbital magnetism

It has been proved that electron saturation effects could affect the correct determination of orbital moments by the XMCD sum rules [29]. Nevertheless, previous calibration experiments performed with the same setup in our group were able to derive the correct orbital and spin moments for bulk Fe, Co, and Ni by using $L_{2,3}$ XMCD. This allows us to interpret the anomalous increase in the orbital to spin moment ratio observed in Fe/InAs(100) interfaces. Similar effects were already reported on ultrathin magnetic films grown on metal substrates [33]. Particularly, for Fe/GaAs(100), an enhancement of 300% of the Fe orbital magnetic moment was recently reported by XMCD [5].

In the present Fe/InAs(100) measurements, the ratio between the orbital and spin moments vary between 6.5% for 3 ML and 19.8% for 1 ML. Note that the bulk Fe shows a value of this ratio of 4.3% [4]. Increased values of the orbital moment are usually connected to (i) the narrowing of the d bands at the surface, causing increased spin moments which enhance the orbital moments by spin-orbit interaction [6]; (ii) the lowering of symmetry which result in reduced crystal field quenching of the orbital moment; and (iii) to the increase of the density of states at the Fermi level [33].

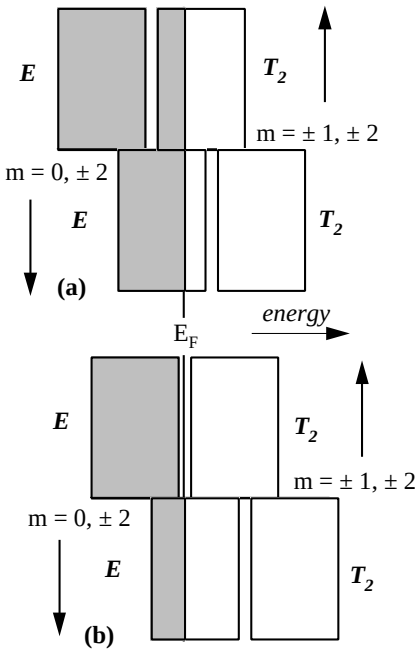

Fig. 7. Spin-polarized Friedel-type density of states, used to compute the orbital moment *via* first-order perturbation theory applied to the spin-orbit splitting term. The shaded areas represent occupied states. (a) represents the model for bulk bcc Fe; (b) the proposed model for Fe/InAs(100), which could explain the enhancement of the orbital moment.

All these effects can appropriately be treated only by first principle theoretical calculations [30,34] which require the complete structural knowledge of the interface. In absence of these data, in the following only a qualitative attempt of explanation for the increase of the orbital moment will be given.

The orbital momentum of bulk bcc Fe is $0.085 \pm 0.08\ \mu_B$ [4]. The present data have shown an orbital momentum as large as $0.22 \pm 0.02\ \mu_B$ for the thickest layer (10 ML of Fe), which is almost three times larger than the value for bulk Fe. A very simple model [35] to explain the orbital magnetism in $3d$ systems starts with a Friedel-type of approximation to $3d$ the density of states (DOS) with two symmetry-adapted type of states, T_2 and E (Fig. 7). The T_2 state is a combination of d wave functions with $m = \pm 1$ and $m = \pm 2$; E is a combination of states with $m = 0$ and $m = \pm 2$. In metal Fe, the majority spin T_2 state is full and the minority spin E state is empty (Fig. 7a). To this (normalized) DOS of total width W_D (around 4 eV for bulk Fe) one applies the spin-orbit interaction in first order perturbation theory. States which are completely full or empty do not contribute to the orbital moment. Note by ζ the spin-orbit coupling constant. Summing over the partial components of the majority E states and of minority T_2 states yields the following

orbital moments (details are given in the work of Eriksson and coworkers [35]):

$$L^{\uparrow} = -\frac{4\zeta}{W_D}\ \mu_B;\quad L^{\downarrow} = \frac{6\zeta}{W_D}\ \mu_B; L^{tot} = \frac{2\zeta}{W_D}\ \mu_B \cdot \quad (5)$$

As a consequence, the orbital moment in bulk Fe is small. Now, we observe that a quantity about three times larger can be retrieved if one just simply supposes that the majority E state is *empty* such that $L^{\uparrow} = 0$. Then, the total orbital momentum has contribution only for minority spin DOS, which is three times larger than the total momentum in bulk bcc Fe.

The situation is represented in Figure 7b. It implies that the Fermi level is located between the T_2 and E states for the majority spin DOS, and that it is located in the T_2 state for the minority spin DOS. This is, of course, valid if the E and T_2 states are separated by an amount exceeding the spin-orbit parameter ζ, which is the case for bcc Fe (see Fig. 1 from Ref. [35]) where this separation exceeds 0.2 eV. In other words, with respect to the case of bulk Fe (Fig. 7a), it seems that the overall filling of the d bands is *lower* in the case of Fe/InAs(100) and this phenomenon is responsible for the increase of the Fe orbital magnetic moment. A possible explanation could be that Fe in coordination with As has a lower $3d$ population due to charge transfer, but one cannot exclude modifications in the Fe $3d$ DOS due to the (neutral) As atoms on top of the Fe layer.

4 Conclusion

The (spin- and orbital-resolved) magnetism of Fe/InAs(100) heterostructures was investigated for the first time, correlated with photoemission analysis of the interface reactivity. All data allowed to support a three-step model of interface formation. In our opinion, the most important result of this study is that Fe deposited on InAs(100) presents ferromagnetic ordering even in the monolayer regime and at room temperature. The orbital moment is unusually high, about three times larger than the orbital moment of bulk bcc Fe. Orbital magnetism is a fascinating but complicated subject; in this work an attempt to explain this increase has been given, starting with a very crude model of DOS and doing the supposition that the $3d$ DOS is depleted due to As, such that the Fermi level separates components with well-defined symmetries in the majority spin DOS. More serious theoretical investigations are needed in the future in order to explain this phenomenon.

The Fe/InAs(100) system seems very promising for spin-injection devices. The carrier mobility in InAs is very high; InAs is a low-gap semiconductor; the Schottky barrier Fe/InAs is low (we did not observe considerable band bending effects in the EDCs while depositing Fe); the Fe MMA stabilizes at a value similar to that of bulk Fe; an interface ferromagnetic compound with the approximate stoichiometry of FeAs is formed; the ratio between orbital and spin magnetism largely exceeds that of bulk α-Fe. As open questions remain the origin of the ferromagnetism in the interface FeAs and possible relationship of it to the structure of the interface layer, as well as the interplay between In islands and metal Fe: are these islands completely free of Fe and As on their top? These phenomena can be investigated by photoelectron diffraction and STM experiments which are planned in the future.

References

1. G.A. Prinz, Science **250**, 1092 (1990)
2. S. Datta, B. Das, Appl. Phys. Lett. **56**, 665 (1990); M. Johnson, R.H. Silsbee, Phys. Rev. B **37**, 5312 and 5326 (1988); M. Johnson, J. Magn. Magn. Mat. **140-144**, 21 (1995)
3. R. Meservey, P.M. Tedrow, R. Fulde, Phys. Rev. Lett. **25**, 1270 (1970); P.M. Tedrow, R. Merservey, Phys. Rev. Lett. **26**, 192 (1971); M.B. Stearns, J. Magn. Magn. Mat. **5**, 167 (1977)
4. P. Carra, B.T. Thole, M. Altarelli, X. Wang, Phys. Rev. Lett. **70**, 694 (1993); C.T. Chen, Y.U. Idzerda, H.-J. Lin, N.V. Smith, G. Meigs, E. Chaban, G.H. Ho, E. Pellegrin, F. Sette, Phys. Rev. Lett. **75**, 152 (1995)
5. Y.B. Xu, M. Tselepi, E. Dudzik, C.M. Guertler, C.A.F. Vaz, G. Wastlbauer, D.J. Freeland, J.A.C. Bland, G. van der Laan, J. Magn. Magn. Mat. **226-230**, 1643 (2001); Y.B. Xu, M. Tselepi, C.M. Guertler, C.A.F. Vaz, G. Wastlbauer, J.A.C. Bland, E. Dudzik, G. van der Laan, J. Appl. Phys. **89**, 7156 (2001)
6. G. van der Laan, Phys. Rev. Lett. **82**, 640 (1999)
7. The reactivity of Fe/GaAs(110) was investigated by core-level photoemission by S.A. Chambers, F. Xuy, H.W. Chen, I.M. Vitomirov, S.B. Anderson, J.H. Weaver Phys. Rev. B **34**, 6605 (1986); however, EDC deconvolutions were not presented in the above reference. For the position of the various reacted components, reference was made to another work done by the same group on Fe/GaAs(110), which presents also deconvolutions of the Ga and As $3d$ core level EDCs: M.W. Ruckman, J.J. Joyce, J.H. Weaver, Phys. Rev. B **33**, 7029 (1986)
8. J.J. Krebs, B.T. Jonker, G.A. Prinz, J. Appl. Phys. **61**, 2596 (1987); A. Filipe, A. Schuhl, P. Galtier, Appl. Phys. Lett. **70**, 129 (1997); B. Lépine, S. Ababou, A. Guirvac'h, G. Jézéquel, S. Députier, R. Guérin, A. Filipe, A. Schuhl, F. Abel, C. Cohen, A. Rocher, J. Creston, J. Appl. Phys. **83**, 3077 (1998)
9. G.W. Anderson, M.C. Hanf, P.R. Norton, Phys. Rev. Lett. **74**, 2764 (1995); E.M. Kneedler, B.T. Jonker, P.M. Thibado, R.J. Wagner, B.V. Shanabrook, L.J. Whitman, Phys. Rev. B **56**, 8163 (1997)
10. Y.B. Xu, E.T.M. Kernohan, D.J. Freeland, A. Ercole, M. Tselepi, J.A.C. Bland, Phys. Rev. B **58**, 890 (1998)
11. Y.B. Xu, E.T.M. Kernohan, M. Tselepi, J.A.C. Bland, S. Holmes, Appl. Phys. Lett. **73**, 399 (1998)
12. W. Mönch, *Semiconductor Surfaces and Interfaces* (Springer, Berlin, 1995)
13. Y.B. Xu, D.J. Freeland, E.T.M. Kerohan, W.Y. Lee, M. Tselepi, C.M. Guertler, C.A.F. Vaz, J.A.C. Bland, S.N. Holmes, N.K. Patel, D.A. Ritchie, J. Appl. Phys. **85**, 5369 (1999)
14. A.T. Hanbicki, B.T. Jonker, G. Itskos, G. Kioseoglou, A. Petrou, Appl. Phys. Lett. **80**, 1240 (2002)

15. M. Tselepi, Y.B. Xu, D.J. Freeland, J. Magn. Magn. Mat. **226-230**, 1585 (2001)
16. Y.B. Xu, D.J. Freeland, M. Tselepi, J.A.C. Bland, Phys. Rev. B **62**, 1167 (2000)
17. C.M. Teodorescu, F. Chevrier, C. Richter, V. Ilakovac, O. Heckmann, L. Lechevalier, R. Brochier, R.L. Johnson, K. Hricovini, Appl. Surf. Sci. **166**, 137 (2000)
18. Y.B. Xu, D.J. Freeland, M. Tselepi, J.A.C. Bland, J. Appl. Phys. **87**, 6110 (2000)
19. J.M. Esteva, R.C. Karnatak, J. Phys. Colloq. France **42**, C2-279 (1984)
20. C.M. Teodorescu, J.M. Esteva, R.C. Karnatak, A. El Afif, Nucl. Meth. Phys. Res. A **345**, 141 (1994)
21. L. Ley *et al.*, in *Photoemission in Solids II: case studies*, edited by L. Ley, M. Cardona (Springer, Berlin, 1979)
22. N.J. Shevchik, J. Tejeda, M. Cardona, Phys. Rev. B **9**, 2627 (1970); M.K. Bahl, R.O. Woodall, R.L. Watson, K.J. Irgolic J. Chem. Phys. **64**, 1210 (1976); K. Hübner, M. Schäfer, Phys. Status Sol. (b) **76**, K63 (1976)
23. H.H. Stadelmaier, M.L. Fiedler, Z. Metallkd. **58**, 633 (1967); C. Dasarathy, Trans. AIME **245**, 1838 (1969)
24. W. Koster, T. Godecke, Z. Metallkd. **68**, 661 (1977)
25. L.A. Clark, Econ. Geol. **55**, 1345 (1960)
26. K. Selte *et al.*, Acta Chem. Scandinav. A **28**, 996 (1974); L.M. Corliss, J.M. Hastings, W. Kunnmann, R.J. Begum, M.F. Collins, E. Gurewitz, D. Mukamel Phys. Rev. B **25**, 245 (1982
27. D.J. Singh, J. Appl. Phys. **71**, 3431 (1992)
28. W.L. O'Brien, B.P. Tonner, Phys. Rev. B **50**, 12672 (1994)
29. R. Nakajima, J. Stöhr, Y.U. Idzerda, Phys. Rev. B **59**, 6421 (1999)
30. R. Wu, A.J. Freeman, Phys. Rev. Lett. **73**, 1994 (1994)
31. C.M. Teodorescu, F. Chevrier, R. Brochier, C. Richter, O. Heckmann, V. Ilakovac, P. De Padova, K. Hricovini, Surf. Sci. **482-485**, 1004 (2001)
32. M. Tanaka, J.P. Harbison, M.C. Park, Y.S. Park, T. Shin, G.M. Rothberg, Appl. Phys. Lett. **65**, 1964 (1994)
33. O. Eriksson, A.M. Boring, R.C. Albers, G.W. Fernando, B.R. Cooper, Phys. Rev. B **45**, 2868 (1992); M. Tischer, O. Hjortstam, D. Arvanitis, J. Hunter Dunn, F. May, K. Baberschke, J. Trygg, J.M. Wills, B. Johansson, O. Eriksson, Phys. Rev. Lett. **75**, 1602 (1995)
34. R. Wu, D. Wang, A.J. Freeman, Phys. Rev. Lett. **71**, 3581 (1993); J. Magn. Magn. Mat. **132**, 103 (1994)
35. O. Eriksson, L. Nordström, A. Pohl, L. Severin, A.M. Boring, B. Johansson, Phys. Rev. B **41**, 11807 (1990)